A Multiscale Attention Mechanism Super-Resolution Confocal Microscopy for Wafer Defect Detection

Xuefeng Sun, Baoyuan Zhang, Yushan Wang, Jialuo Mai, Yuhang Wang, Jiubin Tan, and Weibo Wang

***Abstract*— Confocal microscopy is an essential component of wafer defect detection systems. Wafers are raw materials used in the manufacture of semiconductor chips. The semiconductor chip manufacturing process undergoes frequent updates, which cause an increase in the number and types of defects. This leads to lengthy scanning times for large wafers, and warrants the need to enhance the throughput of optical microscopy inspections. To address this issue, we propose the use of the multi-scale residual dilated convolution attention mechanism network (MRDCAN) super-resolution reconstruction algorithm to reproduce high-resolution images from low-magnification objective lens acquired images. The algorithm introduces the attention mechanism to enhance the information richness of wafer images, introduces the multi-scale expansion convolution to expand the convolutional sensor field to eliminate artefacts to enrich the detailed information of wafer image contours, and meets the image quality requirements through the loss calculation method based on the combination of mean-square error (MSE) and structural similarity (SSIM) image evaluation indices. It is shown that the reconstruction of low-resolution wafer images using this algorithm breaks the optical diffraction limit and achieves the purpose of improving the wafer image resolution. Compared with state-of-the-art models, the proposed algorithm can achieve the best performance with an SSIM index of 94.26 percent for the reconstructed super-resolution wafer images. Our algorithm provides fresh insights into the current challenges of confocal microscopy in the field of wafer defect detection.**

***Note to Practitioners*—Shrinking semiconductor wafer sizes and increasingly complex inspection steps lead to reduced throughput of optical microscope inspection systems. Current convolutional neural network (CNN) networks cannot solve the problem of super-resolution of complex wafer images well. This seriously affects their application in practical detection. Compared with other algorithms, the super-resolution reconstruction algorithm proposed in this paper has a short training time and a multi-scale structure that effectively prevents the loss function curve from oscillating. And the reconstructed wafer image achieves obvious advantages in terms of visual effect and evaluation indices, with strong robustness to Gaussian noise. In addition, the final discussion shows that high-resolution images can be reproduced through the combination of low-magnification objective lens and deep learning super-resolution algorithm, which can simplify the steps of wafer defect detection and increase the efficiency of the whole wafer defect detection by more than 100%. This study demonstrates the potential of super-resolution confocal microscopy for wafer defect detection.**

***Index Terms*— Confocal microscopy, deep learning, super-resolution, wafer defect detection.**

Manuscript received 24 August 2023; revised 15 November 2023; accepted 22 January 2024. This article was recommended for publication by Associate Editor Q. Xu and Editor L. Zhang upon evaluation of the reviewers' comments. This work was supported in part by the National Natural Science Foundation of China under Grant 52275527, Grant 51975161, and Grant 52275526; in part by the Key Research and Development Program of Heilongjiang under Grant 2022ZX01A27; and in part by the China General Nuclear Power Corporation (CGN)-Harbin Institute of Technology (HIT) Advanced Nuclear and New Energy Research Institute under Grant CGN-HIT202201. *(Corresponding author: Weibo Wang.)*

Xuefeng Sun and Baoyuan Zhang are with the Institute of Ultra-Precision Optoelectronic Instrument Engineering and the Key Laboratory of Ultra-Precision Intelligent Instrumentation, Ministry of Industry and Information Technology, Harbin Institute of Technology, Harbin 150080, China (e-mail: 21b301009@stu.hit.edu.cn; byzhang86@163.com).

Yushan Wang and Jialuo Mai are with the Harbin Institute of Technology, Harbin 150080, China (e-mail: wys13634598246@163.com; 1190300213@stu.hit.edu.cn).

Yuhang Wang is with the College of Mechanical and Electrical Engineering, Northeast Forestry University, Harbin 150040, China (e-mail: wangyuhang@nefu.edu.cn).

Jiubin Tan and Weibo Wang are with the Institute of Ultra-Precision Optoelectronic Instrument Engineering, the Key Laboratory of Ultra-Precision Intelligent Instrumentation, Ministry of Industry and Information Technology, and the Advanced Nuclear and New Energy Research Institute, Harbin Institute of Technology, Harbin 150080, China (e-mail: jbtan@hit.edu.cn; wbhit@hit.edu.cn).

Color versions of one or more figures in this article are available at https://doi.org/10.1109/TASE.2024.3358693.

Digital Object Identifier 10.1109/TASE.2024.3358693

I. Introduction

CONFOCAL microscopy is a new instrument developed in recent decades with high light sensitivity and high resolution. It has been widely used in biomedical research and surface analysis of materials science [1], [2], [3]. Wafer defect detection is one of the important application directions of confocal microscopy [4]. In recent years, with the growing popularity and demand for smart phones, tablet computers, smart watches and electronic devices, the semiconductor chip industry has developed rapidly. In addition, the development of the global Internet of Things is still in its infancy. Due to the rapid development of 5G communication, there will be a strong demand for semiconductor chips in the future, as will the construction of other modern and intelligent cities [5]. With the development of these industries, the processing costs and detection efficiency of chips are more demanding, so chip processing technologies are constantly updated, chip

specifications are continuously reduced, and the demand for chips is constantly increasing [6], [7]. As a result, wafer defect detection is continually facing more difficult challenges, and technical innovation is urgently needed [8], [9].

At present, there are various imaging systems for wafer defect detection. The dark-field microscope mainly has a high sensitivity to scratch defect of bare wafer, which is more challenging for patterned wafers [10]. Inspection of wafers using scanning electron microscopy (SEM) requires dozens of defect detection devices per assembly line. This is expensive and does not contribute to the improvement of chip production efficiency. Despite the slower imaging speed of the current state-of-the-art electron beam equipment than the optical imaging, confocal imaging inspection methods continue to be the mainstay of wafer inspection [11], [12], [13], [14]. Wafer inspection using confocal microscopy usually involves two steps, and because the coordinates, area and type of defects estimated from images taken by a confocal microscopy inspection system using a low-magnification objective lens with a wide field of view are subject to error, the defects may not be visible even if an image with the coordinates of the defects is immediately taken using a high-magnification objective lens [15], [16]. In recent years, many methods have been proposed to reduce wafer inspection time. These methods reduce the wafer inspection time from both hardware and software aspects. Van HP et al. proposed a fast scanning acoustic microscope (FSAM) using a slider crank mechanism to expand the scanning area and significantly reduce the wafer inspection time [17]. Wen et al. proposed the use of deep learning methods to improve the speed of wafer defect recognition and shorten the wafer detection time. This method can reduce the defect detection time by 80% compared to the previous method of manual sampling to detect defects [18], [19]. However, with the development of deep learning defect detection algorithms, the defect detection time is gradually difficult to shorten. If the super-resolution algorithm can be applied to the confocal microscope wafer defect detection, the image acquired by the low-magnification objective lens can be used to reproduce the image acquired by the high-magnification objective lens, improve the wafer image resolution to increase the field of view of imaging, and reducing the necessary wafer defect detection steps by half and shortening the detection time from the original duration twofold while significantly enhancing the wafer's defect detection efficiency. The super-resolution algorithm reduces expenses and saves time in the inspection of wafers compared to hardware-based alternatives, making it an advantageous solution for both budget and efficiency.

The emergence of deep learning provides solutions to the above problems to a certain extent. Deep learning super-resolution algorithms mainly use neural networks to learn detailed information such as contours and textures in high-resolution images to reproduce high-resolution (HR) images from low-resolution (LR) images. There are various super-resolution algorithms based on deep learning, among which the algorithm based on convolutional neural network (CNN) and residual networks is the most widely used [20], [21], [22], [23], [24]. Dong C et al proposed the super-resolution reconstruction convolutional network (SRCNN) algorithm and the faster super-resolution reconstruction convolutional network (FSRCNN) algorithm [25]. Zhang et al. proposed the VDSR-f2ILT algorithm to integrate the training of the network and the importance at the pixel level in a common framework [26]. Zhang et al. proposed Image super-resolution using very deep residual channel attention networks (RCAN) algorithm [27]. Song et al. proposed AdderNets that use addition to compute the output features, avoiding the massive energy consumption of traditional multiplication [28]. There are currently several super-resolution algorithms available, although they do not provide satisfactory results when reconstructing images with complex information. Therefore, the prompt reconstruction of such images represents a significant current challenge.

Based on the potential and advantages of deep learning super-resolution reconstruction algorithm in the field of microscopic images [29], [30], we propose the MRDCAN super-resolution reconstruction algorithm to improve the resolution of confocal microscopy images [31], [32]. MRDCAN uses multi-scale dilated convolution to learn the image features of HR images, and the attention mechanism assigns more weight to the feature images with rich information. Feature images with different receptive field sizes of LR images can be extracted directly without increasing the training parameters. In the network, the minimum convolution kernel is used to cascade more convolution layers to accelerate the iterative convergence of the network [33], [34], [35]. The convolution zero filling of the MRDCAN ensures the matching of the input and output sizes. The learnable pixel shuffle layer performs multi-channel recombination of feature images to obtain super-resolution images [36]. The assessment of image quality metrics, such as SSIM, MSE, and peak signal-to-noise ratio (PSNR), plays a vital role in determining the accuracy of defect detection in reconstructed wafer images. These metrics serve as crucial indicators of the effectiveness of super-resolution wafer image reconstruction. Enhanced SSIM and PSNR lead to more pronounced defect visibility in the reconstructed wafer images, minimizing noise and artifacts [37], [38], [39]. Consequently, this results in a heightened accuracy in detecting defects. Moreover, the MRDCAN algorithm makes use of SSIM and MSE of the reconstructed image as the loss function. This helps in promoting network convergence while also reducing the network training time.

The contribution of this paper can be summarized into three points. Firstly, we propose the MRDCAN super-resolution algorithm to improve the wafer image resolution. This is an image resolution enhancement tool, which can quickly improve the wafers image resolution by learning HR wafers image information through training. Secondly, this study demonstrates that the use of the MRDCAN algorithm can result in the reconstruction of wafer confocal microscopy images with large-field-of-view. This, in turn, reduces the number of wafer inspection steps and shortens the inspection time. Therefore, this method can be beneficial in enhancing the defect detection speed. Our MRDCAN algorithm, trained to reconstruct images captured by wafer confocal microscopy, enabled us to attain an SSIM index of up to 94.26%. As a result, the impact of image quality on the precision of defect

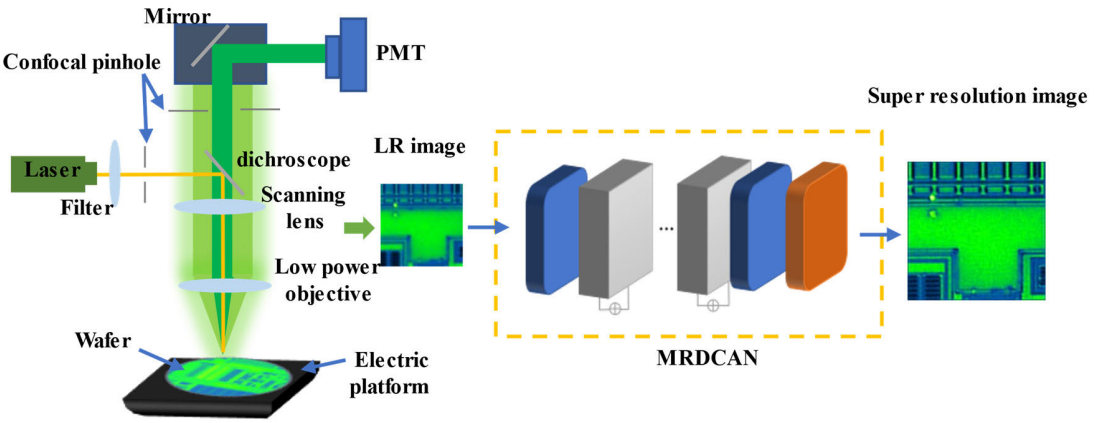

Fig. 1. Structure of a super-resolution confocal microscopy.

detection was minimized. Thirdly, the attention mechanism module is the key module of MRDCAN. We replace the ordinary convolutions in the module with multi-scale dilated convolution, which enables the attention mechanism module to extract feature images at different receptive field scales, effectively improving the image quality of wafer reconstruction without adding any training parameters.

II. Related Work

Deep learning super-resolution algorithms have the ability to reconstruct images end-to-end and have been widely used to solve microscopy image problems, especially the recovery of fluorescence images, wide-field images, and confocal images with low resolution and signal-to-noise ratio [40], [41], [42]. Wang et al. [43] proposed a cross-modal super-resolution method for fluorescence microscopy, which converts diffraction limit input images into super-resolution images based on generative adversarial networks (GAN) [44]. Nehme et al. [45] Proposed the implementation of super-resolution single-molecule microscopy through deep learning, which is a method to obtain super-resolution images with ultra-fast and accurate parameters. Shah et al. [46] applied deep learning to structural illumination microscopy to provide up to twice the spatial resolution of structural illumination microscopy images. Moreover, deep learning super-resolution algorithms have made significant progress compared to traditional deconvolutional super-resolution algorithms. Our previous work has also demonstrated that super-resolution algorithms can achieve good results in microscopy image processing.

A. Super-Resolution Confocal Microscopy Detection System

For the super-resolution confocal microscopy detection system shown in Fig.1, we first use confocal microscopy to collect LR wafer images, and then transfer the LR images to the trained MRDCAN super-resolution algorithm module. In this module, convolution layer is used to down sample the wafer images, and the processed images are transmitted to the residual module, which is used to decompose and output multi-dimensional feature images with a multi-scale attention mechanism module. Pixel Shuffle Layer uses multi-channel feature images to reconstruct super-resolution wafer images for

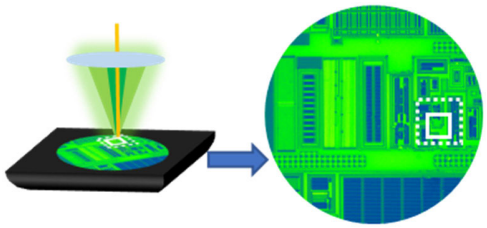

Fig. 2. Image acquisition field with MRDCAN algorithm (dotted area) and without MRDCAN algorithm (solid area).

subsequent processing such as wafer defect location and recognition. Image resolution is closely related to image information richness, and enhanced wafer confocal image resolution also enriches image information. As shown in Fig. 2, we expanded the single image acquisition area and used the super-resolution reconstruction algorithm to increase the image resolution, reduce the number of acquisition and inspection images per wafer, and achieve rapid inspection of wafers. Therefore, the MRDCAN is added to the confocal microscopy wafer detection system to improve the wafer image quality, so that the confocal microscopy high -magnification objective lens can be replaced by the low-magnification large-field objective for wafer detection, thus achieving the purpose of improving the imaging speed and defect detection rate. Moreover, since the super-resolution confocal microscopy does not require any hardware modifications, it can also be applied to any other optical microscopy, such as phase difference microscopy, polarizing microscopy and dark field microscopy [47].

III. Proposed Method–MRDCAN

In the actual wafer defect detection, the structure of the collected wafer image is complex, so it is necessary to design a special network module to solve the problems of uneven distribution of image feature learning weight and serious overfitting of part of the wafer image information during wafer image training. We propose the MRDCAN algorithm based on RCAN. As shown in Fig. 3, the method proposed by us consists mainly of three parts: the shallow feature extraction module, the residual module and the pixel shuffle module.

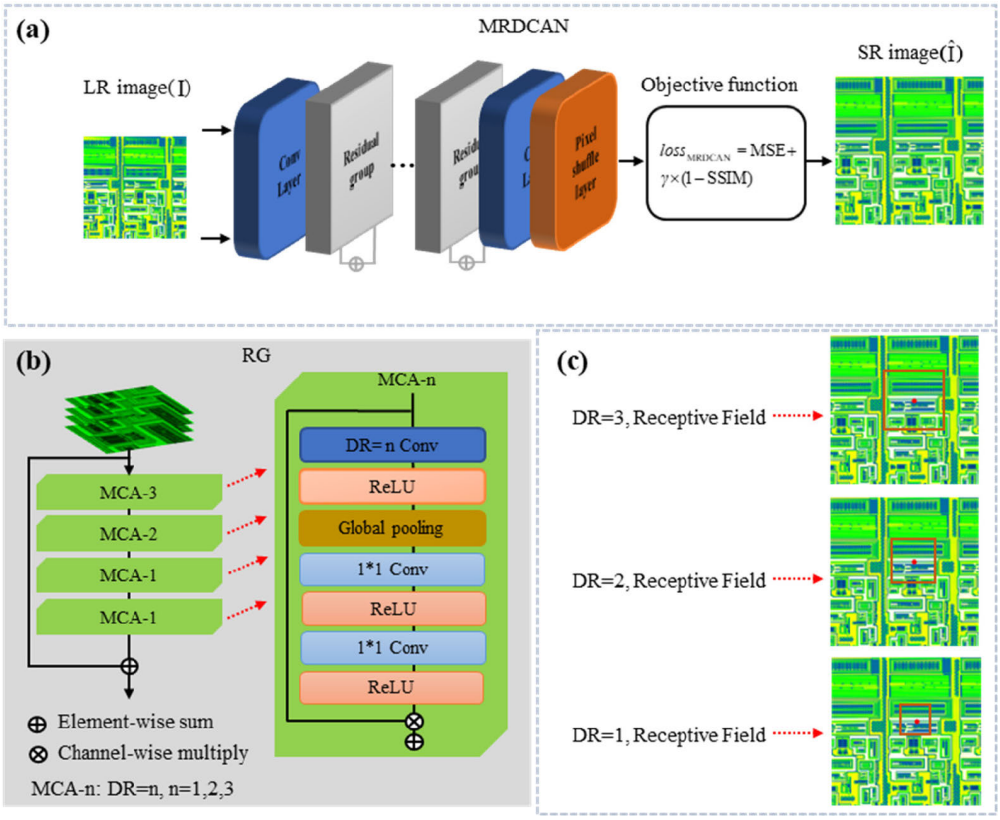

Fig. 3. MRDCAN algorithm structure; (a) Overall network structure; (b) RG network structure; (d) Multiscale dilated convolution receptive fields.

A. Feature Extraction

We use the wafer LR and HR as the training inputs for the MRDCAN algorithm, denoted by I_{L} and I_{H}. SR denotes the output super-resolution image, denoted by I_{SR}. As studied in literature [25] (shown in Fig. 3 (a)), the network in his paper only uses a common convolution layer to extract shallow feature F_1 from input LR image I_{L}:

$$F_1(x_i, y_j) = \mathrm{Conv}_a(I_{\mathrm{L}}(x_i, y_j)) \tag{1}$$

In (1), Conv_a represents the convolution operation, x_i, y_j represents the feature image pixel, and F_1 is the shallow feature extraction for residual module.

The attention mechanism can be considered as a type of guidance, and the attention network can be regarded as a sort of resource redistribution, which can allocate a larger weight to the part with the largest information in the input image, so as to make our training target more accurate [48]. In the process of image reconstruction, features from high frequency channels are also essential for super-resolution reconstruction. Accordingly, the designed network introduces the attention mechanism, which can pay additional attention to such channel features and adjust channel weight adaptively through the interdependence between feature channels. Dilated convolution is a recent convolution proposed for image resolution reduction and information loss caused by down sampling [49], [50]. In addition to enhancing resolution, dilated convolution also widens the scope of the convolution kernel to include additional image information, which is profitable for eliminating image artifacts and obtaining image details.

As shown in Fig. 3(a), in order to achieve super-resolution reconstruction of the wafer image, The network structure of this paper uses six residual groups (RG) to build residual modules. The residual module can increase the depth of the two-dimensional convolutional network and provide additional network parameters, so that the network can obtain abundant details of the wafer image, which is conducive to learning its image features. The attention mechanism, which is similar to human vision, can globally scan the image to obtain the target regions that need to be focused, thus reconstructing the wafer super-resolution image more accurately. We improved the network by upgrading the multi-channel attention (MCA) in RG, as shown in Fig. 3 (b). Each RG contains four MCA-n with dilated convolution kernels of different scales n represents the dilated rate (DR) in the dilated convolution, and DR = n represents the convolution receptive fields of different scales, as shown in Fig.3(c). We also add a long-hop link structure to the MCA-n module to extract statistics between channels and further enhance the discriminative power of the network on the wafer image. Wafer image features extracted from the residual module as follows:

$$\begin{aligned} F_{\mathrm{RG}}^{1}(x_i, y_j) = {} & \mathrm{MCA1}(\mathrm{MCA1}(\mathrm{MCA2}(\mathrm{MCA3} \\ & (F_1((x_i, y_j)))))) + F_1(x_i, y_j), \end{aligned} \tag{2}$$

$$\begin{aligned} F_{\mathrm{RG}}^{m}(x_i, y_j) = {} & \mathrm{MCA1}(\mathrm{MCA1}(\mathrm{MCA2}(\mathrm{MCA3} \\ & (F_{\mathrm{RG}}^{m-1}(x_i, y_j)))))) + F_{\mathrm{RG}}^{m-1}(x_i, y_j) \\ & m = 2, 3, \cdots, 6. \end{aligned} \tag{3}$$

MCA2 and MCA3 represent the dilated convolution with DR = 3 and DR = 2, MCA1 (DR = 1) represent the

traditional convolution. The multiscale dilated convolution is added to the MCA module, which can provide receptive fields of multiple scales, so that the network can learn more detailed information in image I_{L}. The feature parameter F_{RG}^{6} output by the residual module is input to the pixel module Pixels Shuffle layer through the GRLU activation layer to obtain H_{PS}. Pixels Shuffle layer is different from the traditional interpolation algorithm to reconstruct images, but it obtains HR images by learning and fusing multi-channel feature images. Through the convolutional layer and Sigmoid activation layer, the image is enlarged to the ground truth image size. Ultimately, the single-channel super-resolution image I_{SR} is output:

$$I_{SR}(x_i, y_j) = \mathrm{Cov}(\mathrm{H_{PS}}(\mathrm{Cov}(F_{\mathrm{RG}}^{6}(x_i, y_j)))) \tag{4}$$

B. Network Loss Function

In the network, we use the loss function to measure the difference between super- resolution wafer images and HR wafer images. The less loss value we get, the more accurate the forecast will be. In deep learning, we need to minimize the loss function through training data to determine parameter values. The loss function of MRDCAN algorithm mainly adopts the combination of mean square error (MSE) and structural similarity. MSE can ensure the accuracy of network learning and training and reasonably control the dynamic range of network prediction. SSIM enhances the structural similarity of the output images. It is of great significance to use the two image evaluation indexes as the loss function of MRDCAN, which can evaluate the overall performance of the wafer image, such as the brightness, the similarity structure degree to the HR wafer image and the gray level error, and finally generate the evaluation matrix.

$$\mathrm{MSE}(\hat{I}, I) = \sqrt{\frac{1}{h \times w} \sum_{i=1}^{h \times w} (I_i - \hat{I}_i)^2} / (\max(I) - \min(I)) \tag{5}$$

$$\mathrm{SSIM}(\hat{I}, I) = [l_M(\hat{I}, I)]^{\alpha_M} \prod_{z=1}^{M} [c(\hat{I}, I)]^{\beta_z} [s(\hat{I}, I)]^{\gamma_z} \tag{6}$$

$$Loss_{MR} = \mathrm{MSE}(\hat{I}, I) + (1 - \mathrm{SSIM}(\hat{I}, I)) \tag{7}$$

where $l_M(\hat{I}, I)$, $c(\hat{I}, I)$ and $s(\hat{I}, I)$ are brightness similarity, contrast similarity and structure similarity corresponding to scale Z, respectively. The corresponding exponents a_M, β_z, γ_z are used to adjust the weight of the three parts, typically taking $a_z = \beta_z = \gamma_z$, $\sum_{z=1}^{M} \gamma_z = 1$.

C. 2,3-RDCAN, RCNA and FSRCNN

The receptive fields of the feature images extracted by the dilated convolution at different scales are different, which will affect the training results of the network. Therefore, we have designed single scale networks with DR = 2, 3: 2-RDCAN and 3-RDCAN. The aim is to demonstrate that the MRDCAN algorithm architecture with multi-scale cavity convolution has the greatest advantage and best performance in improving the wafer image resolution. The main difference between them and MRDCAN algorithm structure is that the dilated convolution Din RG is different. We constructed 2-RDCAN and 3-RDCAN with DR = 3 and DR = 2 dilated convolution (Fig. 4 (a-b)). The above two networks were trained with the same training parameters and image preprocessing steps as MRDCAN. In addition to the aforementioned networks, the study also incorporates the FSRCNN network, as depicted in Fig. 4(d), and the RCAN network. The RCAN network, specifically detailed in Fig. 4(c), comprises 50 RG modules. This setup is crucial for validating the superior capabilities of the MRDCAN network in reconstructing super-resolution wafer images. By comparing these four distinct network model structures and assessing the quality of the generated super-resolution images of the wafers, the study aims to highlight the efficacy and advantages of the multi-scale proof MRDCAN network.

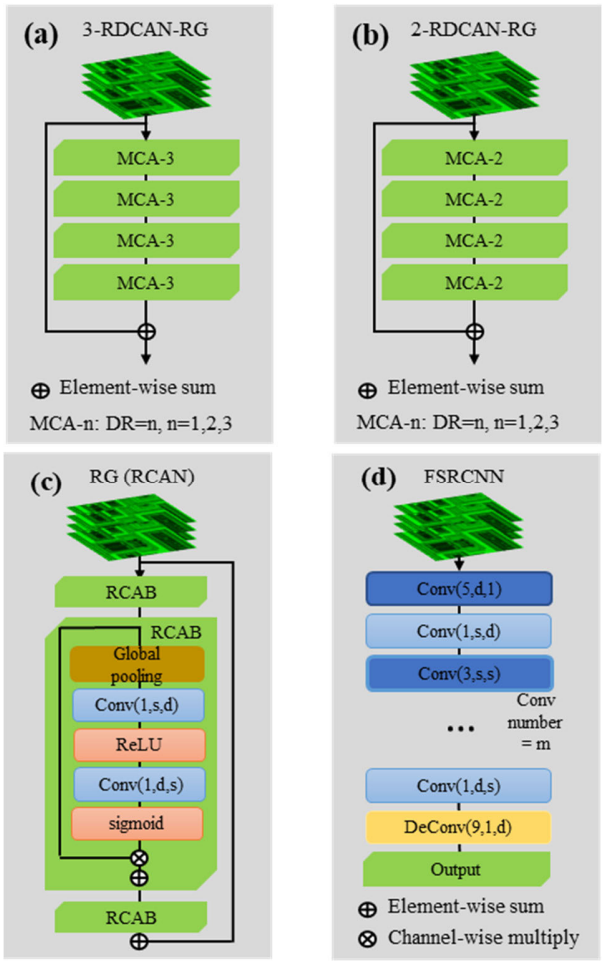

Fig. 4. (a) Single scale residual structure (DR = 3):; (b) Single scale residual structure (DR = 2); (c) RG module architecture of RCAN networks (RCAB: Residual channel attention blocks, d and s are the number of convolution kernels and the number of channels); (d) FSRCNN network architecture.

IV. Data Set Preparation and Network Training

A. Data Set Preparation

We used an industrial confocal microscopy to capture wafer images to make the dataset. The target wafer size is 12 inches, which is the most common size in wafer processing today. The confocal microscopy is composed of a confocal imaging scanning system, electron optics system, and microcomputer

image analysis system with ultra-high spatial resolution and sensitivity. Wafer images are captured using an Olympus OLS5000 microsystem, which uses a computer-controlled scanning algorithm for 3D imaging. A 405-nm laser diode light source and a high-sensitivity photomultiplier tube are used to obtain confocal images up to 120nm. The wafer image data were collected using a 50x low-magnification objective lens and a 100x high-magnification objective lens (MPLAPON50xLEXT, MPLAPON100xLEXT) with a numerical aperture (NA) of 0.95 and a working distance of 0.35mm. In order to reduce the workload of image preprocessing, the validation set and training set of the dataset were collected separately: (1) 500 high-resolution images (1024×1024 pixels) containing various defects were collected with 100x objective to make the training set; (2) Use the 50x objective to capture a wafer image, switch to the 100x objective without moving the stage, obtain a 100x wafer image of a small field of view within the 50x objective field of view. Use the SIFT feature matching registration method to find overlaps. Due to the high similarity of wafer feature points, it is difficult to register images. We use manual cropping to select feature areas and obtain 50 image pairs (1024 ×1024 pixels) to make a network verification set. The LR images in the training set are obtained by degrading the HR images using the cubic linear interpolation algorithm. The specific operation is to use the cubic interpolation algorithm to interpolate the 1024 × 1024 HR image to 256×256 pixels and then to 512×512 pixels to obtain the LR image. Because low-resolution images are interpolated from HR images, image pairs in the training set do not need to be registered, which reduces the workload of image registration and improves the robustness of the network.

Deep learning research has found that the size of the data set has a significant impact on network performance. The richer the wafer defect information contained in the produced data set, the final training effect will be closer to the real image. In order to obtain sufficient data sets, we expanded the collected wafer images. The main processing methods were 90°, 180° and 270° rotation and random cropping of the collected images. The final dataset contains 25000 wafer image pairs (256×256 pixels and 128×128 pixels), including 22,000 images in the training set and 3000 images in the validation set.

B. Experimental Environment

The MRDCAN algorithm and other comparison test algorithm experiments are completed in the dell tower 7920 workstation. The workstation is equipped with NVIDIA GeForce GTX 3090 GPU, dual Inter Core 4210R CPU @ 2.6ghz and 128G running memory. The software environment is ubuntu18.04, CUDA Toolkit 11.4, CUDNN8.0, NviDIa-TensorFlow1.15.0 and Python3.6. This software configuration enables TensorFlow to run in higher version CUDA, which can fully play the performance of the 3090 graphics card and improve network training efficiency.

C. Network Training

In this work, we primarily train the MRDCAN algorithm with a training dataset consisting of 25,000 image pairs.

TABLE I
NETWORK TRAINING TIME

	RCAN	3-RDCAN	2-RDCAN	FSRCNN	MRDCAN
Time (hour)	14	11.4	10.5	10.3	10.6

In the process of network training, we use the computationally efficient Adam optimizer with a small memory footprint according to the scale of network parameters. This optimizer can replace the traditional stochastic gradient descent algorithm by updating the weights based on the trained image data. We set the training batch size between 4 and 16, depending on the size of the network training images and the running memory size of the computer GPU. Initial training requires randomly initializing the network model and starting the network training with a learning rate of 10^{-4} with a decay factor of 0.5. As the network is trained continuously, the minimum decay rate can be 10^{-5}. When the learning rate is set above 10^{-4}, some of the networks are trained to overfit and the reconstructed super-resolution wafer images are distorted. For testing, in order to maintain the highest learning rate, the best performance of the network training, and to prevent overfitting of the network training, we set the number of network iterations to 20, 000, which took a total of 10.6 hours and only 0.05 seconds to reconstruct the wafer super-resolution image.

To demonstrate the universality and effectiveness of the MRDCAN in improving the resolution and structural similarity of wafer super-resolution images. With consistent training parameters, we also trained RCAN, FSRCNN, 3-RDCAN, 2-RDCAN and MRDCAN networks for comparison with our algorithm.

Table I shows the time required to train the different five networks. Except for RCAN, the training time for several other networks is largely the same. Fig.5 shows the loss function curves of our trained networks, from the graphs we can see that there is a big difference in the loss function curves for training complex wafer images using different networks. The loss function curve of the MRDCAN algorithm shows a stepwise and gentle decrease with fast convergence. The loss function curve of FSRCAN fluctuates drastically in the magnification range, which is not favourable for network training. The loss function curves of RCAN and the single scale networks (3-RDCAN) have large fluctuations in the loss curves due to the complexity of the wafer image features.

V. EXPERIMENTAL RESULTS AND DISCUSSION

In this section, we present the wafer images reconstructed by MRDCAN and other advanced super-resolution algorithms, and analyze the evaluation index results of the reconstructed super-resolution wafer images. Moreover, we test the Gaussian noise robustness of MRDCAN. In the experimental analysis in this section, the same preprocessing algorithm is adopted for all test images, and training tests are completed on the same workstation to ensure the objective and fair results.

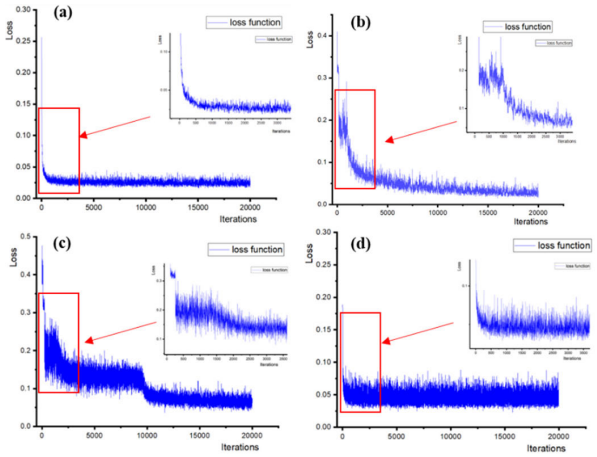

Fig. 5. (a) MRDCAN Loss function curve; (b) FSRCNN Loss function curve; (c) RCAN Loss function curve; (d) 3-RDCAN Loss function curve.

A. MRDCAN Reconstruction Results

In Fig. 6, We demonstrate the image of wafer with solder joint defects reconstructed by MRDCAN algorithm. Fig.6 (b-d) shows the HR wafer image, the LR wafer image, and the super-resolution wafer image reconstructed by MRDCAN algorithm. Fig.6 (e-g) shows the enlarged images in the dashed frame of (b-d) and compares the resolution of the reconstructed image defects. From the local magnified image and evaluation index analysis, it is evident that the defect profile of the super-resolution image reconstructed by the MRDCAN algorithm is lucid. Furthermore, the cross-sectional curve of the defect exhibits the closest resemblance to that of the defect in the high-resolution image. It is proved that it is feasible to use low-magnification objective lens instead of high-magnification objective lens to increase the imaging field of view and improve Improved image resolution. Note that all network output images shown in this paper are blindly generated by deep learning.

The distributions for the SSIM values of the test data for network input images and network output images are shown in Fig. 6 (h-i) (The test dataset has a total of 100 wafer images). The X-coordinate in the figure shows identical two values. The unfilled circle represents the evaluation metric of the low-resolution input image, whilst the filled circle represents the evaluation metric of the super-resolution image generated. The reconstructed wafer images by the MRDCAN algorithm show a mean SSIM value of 0.886 and a mean PSNR value of 25.852. Research documented in literature [37] reveals a direct positive relationship between the SSIM and PSNR values of defective images and their defect detection accuracy. Notably, a defect detection accuracy of 97% is achievable when the SSIM value approximates 0.850 and the PSNR approximates 25.000. Furthermore, the accuracy remains impressively over 90% even if the SSIM value drops to 0.759. This performance aligns well with the prevailing standards for basic inspection in wafer defect detection.

B. Reconstruction Results of Multiple Super-Resolution Algorithms

This paper also compares the MRDCAN algorithm with other advanced super-resolution algorithms. The reconstruction results of different algorithms for wafer image are shown in Fig. 7. Fig.7 (c-e) displays the example images of the super-resolution wafer reconstructed using RCAN, FSRCNN, and the MRDCAN algorithm. Compared with wafer image reconstructed by traditional interpolation algorithm (Fig. 7(b)). The resolution of the wafer image reconstructed by the three super-resolution algorithms has been greatly improved. Fig.7 (f-j) is the corresponding local enlarged image in the virtual box. Compared with the latter two reconstruction algorithms, the wafer image reconstructed by the RCAN reconstruction algorithm has poor resolution. The resolution of wafer images reconstructed by FSRCNN and MRDCAN is difficult to distinguish. Therefore, we insert two commonly used image assessment indexes, SSIM and PSNR, for quantitative analysis of reconstructed images. Table II presents the mean evaluation metrics of 100 sets of images that were reconstructed using the MRDCAN algorithm and other super-resolution reconstruction algorithms. Compared with the wafer image reconstructed by the traditional cubic interpolation algorithm, the SSIM index is increased by 73.04%, and the PSNR index is increased by 28.47%. Compared with RCAN and FSRCNN, the PSNR index increased by 16.27% and 10.32%, and the SSIM index increased by 21.02% and 7.13%. In addition to the evaluation parameters mentioned above, the reconstruction time parameters are also excellent. Although MRDCAN has a greater number of network depth and parameters than FSRCNN, the reconstruction time is almost identical. Based on the observation and analysis of the image evaluation index results, it can be concluded that the MRDCAN algorithm produces a higher resolution wafer image than other algorithms.

TABLE II
EVALUATION RESULTS OF SUPER-RESOLUTION RECONSTRUCTION IMAGES

	Bicubic	RCAN	FSRCNN	MRDCAN
SSIM	0.512	0.732	0.827	**0.886**
PSNR	20.123	22.235	23.432	**25.852**
TIME	0.13	0.080	**0.051**	**0.052**

C. Advantages of MRDCAN for Multi-Scale Dilated Convolution Structure

In order to verify that the multi-scale dilated convolution structure has a higher resolution than the single-scale dilated convolution structure in the reconstruction of the wafer image. We trained 3-RDCAN, 2-RDCAN single scale network and MRDCAN multi-scale networks super-resolution reconstruction algorithms. The defect wafer image reconstructed by the three super-resolution algorithms is shown in Fig. 8. We compared the reconstructed three wafer images in Fig. 8(c-e) with the input LR Fig. 8(b). The resolution of the three reconstructed images was much superior than that of the input images, and the reconstructed image clarity of our MRDCAN algorithm was higher than that of the other two algorithms. The local magnified Fig. 8(h-j) of the wafer image reconstructed by the three algorithms shows the details of the

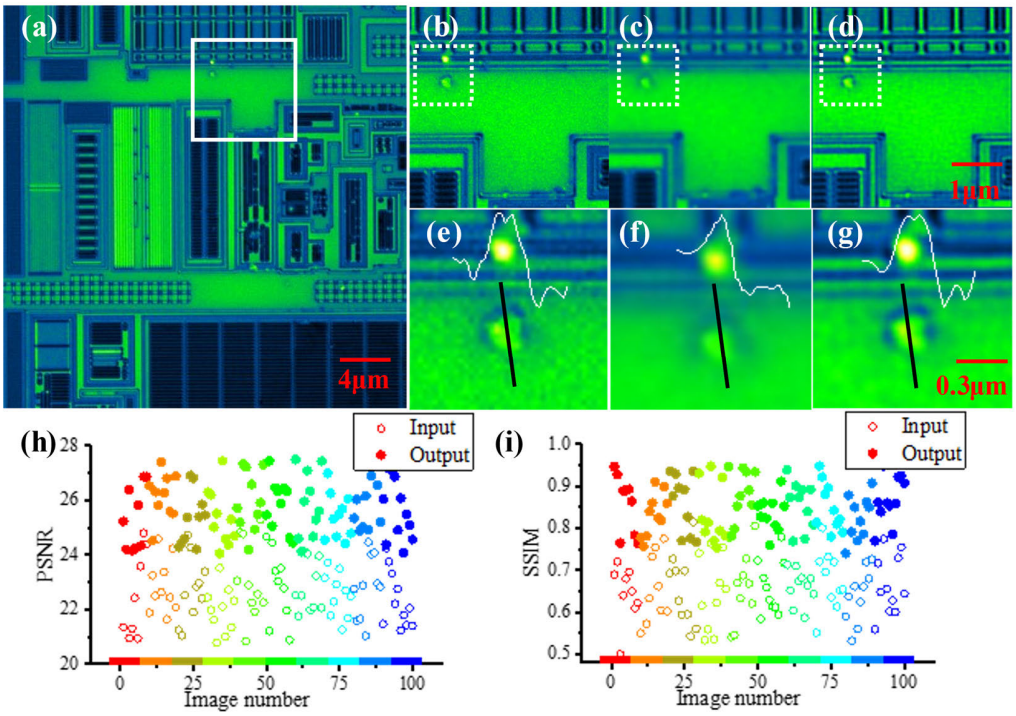

Fig. 6. Image reconstruction results of MRDCAN wafer defects; (a) A large FOV wafer image captured by 50x objective; (b) HR wafer image captured by 100x objective; (c) LR wafer image captured by 50x objective; (d) Network output super-resolution wafer image; (e-g) Magnified images of the ROIs in the white box of (b-d); (h-i) Distribution for PSNR and SSIM values of network input images and network output images in test dataset. The pixel value of the cross section of the wafer defects is represented by the white curve.

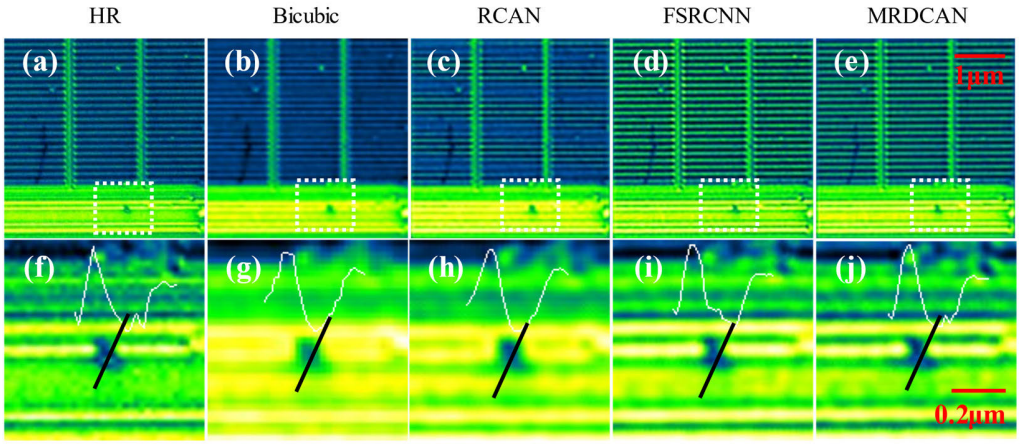

Fig. 7. Multiple super-resolution algorithms for image reconstruction; (a) HR wafer image captured by 100x objective; (b) Image reconstructed by Bicubic algorithm; (c) Image reconstructed by RCAN algorithm; (d) Image reconstructed by FSRCNN algorithm; (e) Image reconstructed by MRDCAN algorithm; ((f- j) Magnified images of the ROIs in the white box of (a-e). The pixel value of the cross section of the wafer defects is represented by the white curve.

TABLE III
EVALUATION RESULTS OF WAFER SUPER-RESOLUTION RECONSTRUCTION IMAGES BY DIFFERENT ALGORITHMS

	LR	3-RDCAN	2-RDCAN	MRDCAN
SSIM	0.597	0.687	0.664	**0.731**
PSNR	24.446	26.081	25.245	**26.932**

reconstruction algorithm. It can be observed that the wafer image reconstructed by MRDCAN algorithm can better reconstruct the details of defects. Simultaneously, the SSIM and PSNR evaluation indices of the four groups of reconstructed wafer images (Table III) were assessed quantitatively. The SSIM of the wafer image, reconstructed using the MRDCAN algorithm, increased by 22.45% compared to that of the LR image. Compared with 3-RDCAN (DR=3) and 2-RDCAN (DR=2) single scale network, the SSIM index of wafer images reconstructed by MRDCAN algorithms increased by 6.40% and 10.09% respectively. Compared with the LR image, the PSNR index of the reconstructed wafer images by the three algorithms is respectively increased by 10.17%, 6.68% and 3.26%, which fully proves the advancement of the proposed algorithm. These robust results indicate that multiple dilated convolution structure networks are the most suitable choice for wafer image reconstruction.

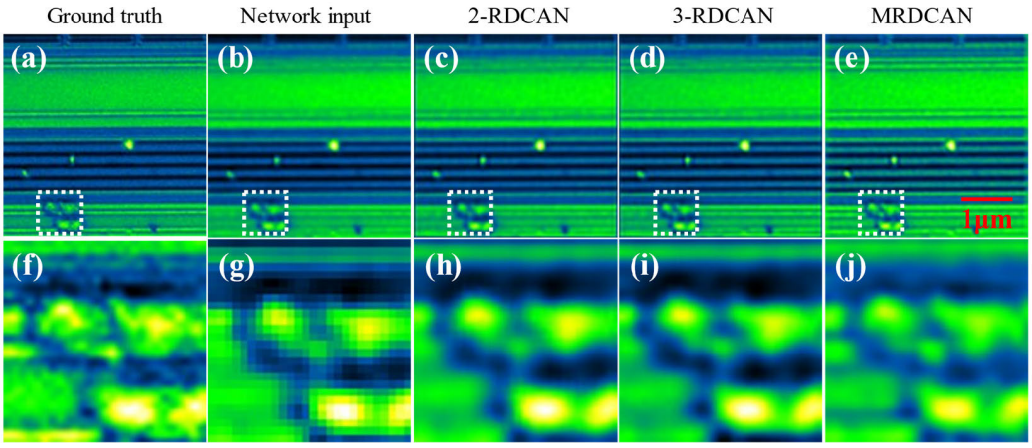

Fig. 8. Super-resolution reconstruction results of multi-scale dilated convolution networks; (a) HR wafer image captured by 100x objective; (b) LR wafer image captured by 50x objective; (c) 2-RDCAN reconstruction of wafer image; (d)3-RDCAN reconstruction of wafer image; (e)MRDCAN reconstruction of wafer image; (f-j) Magnified images of the ROIs in the white box of (a-e).

TABLE IV
EVALUATION RESULTS OF WAFER SR RECONSTRUCTED IMAGES WITH DIFFERENT LEVELS OF NOISE

	LR	LR+GN0.001	LR+GN0.002	LR+GN0.005	LR+GN0.01
SSIM	0.731	0.589	0.576	0.442	**0.328**
PSNR	25.556	24.6325	22.891	19.432	**19.213**
	HR	SR(GN0.001)	SR(GN0.002)	SR(GN0.005)	SR(GN0.01)
SSIM	--	0.762	0.759	0.689	**0.615**
PSNR	--	27.132	25.532	22.985	**21.302**

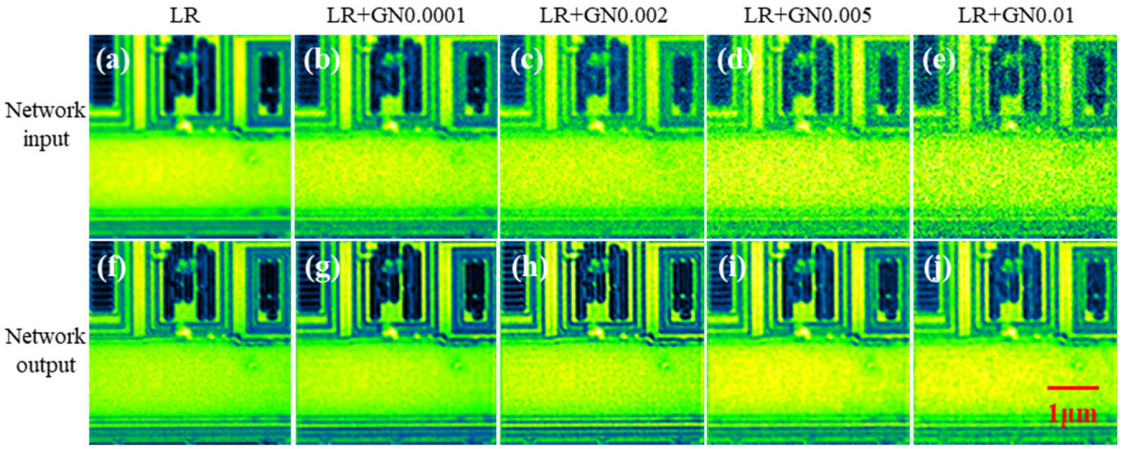

Fig. 9. Reconstruction results of MRDCAN algorithm under different noise intensity; (a) LR image captured by 50x objective; (b-e) LR images with different degrees of Gaussian noise; (f) HR image captured by 100x objective; (g-j) are reconstructed super-resolution images of the wafer corresponding to (b-e).

D. The Generalization Capability of the Proposed Method-MRDCAN

Due to different imaging conditions, the acquisition of wafer images will produce various noises that cannot be avoided, among which the gaussian white noise introduced by image sensors and circuit components is the most common [51], [52]. In order to verify the robustness of the proposed MRDCAN algorithm in dealing with Gaussian noises of various intensities, Gaussian noises (GN) with noise level variance $\sigma = 0.001$, 0.002, 0.005 and 0.01 were added to the LR images of network input, as shown in Fig. 9 (b-e). We can obviously see from the reconstruction result image Fig. 9 (g-j) that the reconstruction results with different noises have achieved excellent results. As shown in the evaluation results in Table IV, when the noise level variance is $\sigma = 0.001$ and $\sigma = 0.002$, the SSIM index of the reconstructed super-resolution image is very close. As the noise level increases, the SSIM index of the reconstructed wafer image by MRDCAN gradually decreases from 0.762 to 0.615. However, compared with the LR image, the SSIM index of the reconstructed wafer image increases from 29.3% to 87.5%, indicating that the more GN the MRDCAN algorithm improves the resolution of the wafer image, the more obvious it is. It is proved that the MRDCAN algorithm is robust to GN.

VI. Conclusion

This paper focuses on the limitations of the current confocal microscopy for detecting wafer defects with low efficiency. To address this issue, the study employs a low-magnification objective and super-resolution algorithm, resulting in the production of high-resolution wafer confocal images. This enhances wafer detection throughput and improves wafer defect detection efficiency. And the MRDCAN super-resolution reconstruction algorithm is proposed to enhance the resolution of low-magnification objectives. The objective is achieving high-resolution imaging with a large field of view. The reconstructed images of the MRDCAN algorithm were analysed alongside various other advanced super-resolution algorithms, and the results showed that MRDCAN performed best for reconstructing wafer images with complex information. In addition, we also prove that the MRDCAN algorithm has strong Gaussian noise robustness. It is shown that the MRDCAN algorithm can quickly reconstruct confocal super-resolution images. In experiments, the algorithm has demonstrated an increase of 67% in the resolution of wafer images captured using a low-magnification objective lens, which nearly equals the resolution of those taken with a high- magnification objective lens. Therefore, we use a low-magnification objective lens to reproduce the wafer image collected by a high-magnification objective lens. This technique expands the imaging field of view, decreases the number of steps in wafer defect detection, and ultimately leads to an enhanced detection rate for wafer defects. However, the image super-resolution reconstruction time is only tens of milliseconds, which is negligible compared to the entire wafer inspection time.

The super-resolution microscopy technology in this paper also has shortcomings. The super-resolution deep learning algorithm is to train the neural network to learn the characteristics of high-resolution wafer images, and input the low-resolution wafer images into the trained model to generate super-resolution wafer images. Since our learning goal is a high-resolution wafer image, the final result is only infinitely close to the high-resolution image. The method presented in this paper facilitates the large-scale, rapid detection of wafer defects. Although high-precision wafers still need to be detected by a high-magnification objective lens, the method described in this paper can significantly reduce the workload of high-precision wafer inspection. In this research, we utilised a deep learning network algorithm to improve the confocal microscopy super-resolution technique's efficiency in reconstructing wafer images. Despite the impressive outcome, we only employed a single complex wafer dataset to train the MRDCAN network. If the algorithm is used to reconstruct other complex wafer images, we need to train the network using different wafer datasets. Improving the robustness and transfer learning capability of super-resolution algorithms is also our next research direction. We are optimistic that this progress in fast, high-resolution imaging technology will substantially broaden the applicability of our approach to a more extensive range of optoelectronic inspection devices and inspection domains.

References

[1] S. Usuki, H. Nishioka, S. Takahashi, and K. Takamasu, "Experimental verification of super-resolution optical inspection for semiconductor defect by using standing wave illumination shift," *Int. J. Adv. Manuf. Technol.*, vol. 46, nos. 9–12, pp. 863–875, Feb. 2010, doi: 10.1007/s00170-008-1901-y.

[2] M. Harada, Y. Minekawa, and K. Nakamae, "Defect detection techniques robust to process variation in semiconductor inspection," *Meas. Sci. Technol.*, vol. 30, no. 3, Feb. 2019, doi: 10.1088/1361-6501/aafd7.

[3] J.-C. Chien, M.-T. Wu, and J.-D. Lee, "Inspection and classification of semiconductor wafer surface defects using CNN deep learning networks," *Appl. Sci.*, vol. 10, no. 15, p. 5340, Aug. 2020, doi: 10.3390/app10155340.

[4] J. Zhu et al., "Optical wafer defect inspection at the 10 nm technology node and beyond," *Int. J. Extreme Manuf.*, vol. 4, no. 3, Sep. 2022, Art. no. 032001, doi: 10.1088/2631-7990/ac64d7.

[5] Z. Chen, S. Yan, and C. Danesh, "MicroLED technologies and applications: Characteristics, fabrication, progress, and challenges," *J. Phys. D, Appl. Phys.*, vol. 54, no. 12, Mar. 2021, Art. no. 123001, doi: 10.1088/1361-6463/abcfe4.

[6] Z. Wang, H. Yang, W. Li, and Z. Yin, "Super-resolving IC images with an edge-preserving Bayesian framework," *IEEE Trans. Semicond. Manuf.*, vol. 27, no. 1, pp. 118–130, Feb. 2014, doi: 10.1109/TSM.2013.2293581.

[7] B. M. Barnes, F. Goasmat, M. Y. Sohn, H. Zhou, A. E. Vladár, and R. M. Silver, "Effects of wafer noise on the detection of 20-nm defects using optical volumetric inspection," *J. Micro/Nanolithography, MEMS, MOEMS*, vol. 14, no. 1, Feb. 2015, Art. no. 014001, doi: 10.1117/1.jmm.14.1.014001.

[8] S. Cheon, H. Lee, C. O. Kim, and S. H. Lee, "Convolutional neural network for wafer surface defect classification and the detection of unknown defect class," *IEEE Trans. Semicond. Manuf.*, vol. 32, no. 2, pp. 163–170, May 2019, doi: 10.1109/TSM.2019.2902657.

[9] H. Guo et al., "Imaging nano-defects of metal waveguides using the microwave cavity interference enhancement method," *Nanotechnology*, vol. 31, no. 45, Nov. 2020, Art. no. 455203, doi: 10.1088/1361-6528/abaa74.

[10] J. Huff, "The airyscan detector from ZEISS: Confocal imaging with improved signal-to-noise ratio and super-resolution," *Nature Methods*, vol. 12, no. 12, pp. 1–2, Dec. 2015, doi: 10.1038/nmeth.f.388.

[11] I. Gregor and J. Enderlein, "Image scanning microscopy," *Current Opinion Chem. Biol.*, vol. 51, pp. 74–83, Aug. 2019, doi: 10.1016/j.cbpa.2019.05.011.

[12] R. K. Attota and H. Kang, "Parameter optimization for through-focus scanning optical microscopy," *Opt. Exp.*, vol. 24, no. 13, p. 14915, 2016, doi: 10.1364/oe.24.014915.

[13] S. Purandare, J. Zhu, R. Zhou, G. Popescu, A. Schwing, and L. L. Goddard, "Optical inspection of nanoscale structures using a novel machine learning based synthetic image generation algorithm," *Opt. Exp.*, vol. 27, no. 13, p. 17743, 2019, doi: 10.1364/oe.27.017743.

[14] J. Liu et al., "High-yield, wafer-scale fabrication of ultralow-loss, dispersion-engineered silicon nitride photonic circuits," *Nature Commun.*, vol. 12, no. 1, pp. 1–9, Apr. 2021, doi: 10.1038/s41467-021-21973-z.

[15] A. Ito, A. Miyamoto, N. Kondo, and M. Harada, "Super-resolution method for SEM images based on pixelwise weighted loss function," *Microscopy*, vol. 30, no. 3, Feb. 2023, Art. no. dfad009, doi: 10.1093/jmicro/dfad009/7026008.

[16] M. Harada, Y. Minekawa, and K. Nakamae, "Defect detection techniques robust to process variation in semiconductor inspection," *Meas. Sci. Technol.*, vol. 30, no. 3, Feb. 2019, Art. no. 035402, doi: 10.1088/1361-6501/aafd77.

[17] V. H. Pham et al., "Development of fast scanning module with a novel bubble solution applied to scanning acoustic microscopy system for industrial nondestructive inspection," *Expert Syst. Appl.*, vol. 228, Oct. 2023, Art. no. 120273, doi: 10.1016/j.eswa.2023.120273.

[18] G. Wen, Z. Gao, Q. Cai, Y. Wang, and S. Mei, "A novel method based on deep convolutional neural networks for wafer semiconductor surface defect inspection," *IEEE Trans. Instrum. Meas.*, vol. 69, no. 12, pp. 9668–9680, Dec. 2020.

[19] S. Lei, S. Lu, and K. Yang, "A super-resolution model for improving the precision of wafer mark alignment," *J. Phys., Conf. Ser.*, vol. 1699, no. 1, Nov. 2020, Art. no. 012024, doi: 10.1088/1742-6596/1699/1/012024.

[20] J. Hu, L. Shen, and G. Sun, "Squeeze-and-excitation networks," in *Proc. IEEE/CVF Conf. Comput. Vis. Pattern Recognit.*, Jun. 2018, pp. 7132–7141, doi: 10.1109/CVPR.2018.00745.

[21] C. Ledig et al., "Photo-realistic single image super-resolution using a generative adversarial network," in *Proc. IEEE Conf. Comput. Vis. Pattern Recognit. (CVPR)*, Jul. 2017, pp. 105–114.

[22] C. Belthangady and L. A. Royer, "Applications, promises, and pitfalls of deep learning for fluorescence image reconstruction," *Nature Methods*, vol. 16, no. 12, pp. 1215–1225, Dec. 2019, doi: 10.1038/s41592-019-0458-z.

[23] K. Zhang, J. Liang, L. Van Gool, and R. Timofte, "Designing a practical degradation model for deep blind image super-resolution," in *Proc. IEEE/CVF Int. Conf. Comput. Vis.*, May 2022, pp. 4771–4780, doi: 10.1109/iccv48922.2021.00475.

[24] M. Weigert et al., "Content-aware image restoration: Pushing the limits of fluorescence microscopy," *Nature Methods*, vol. 15, no. 12, pp. 1090–1097, Dec. 2018, doi: 10.1038/s41592-018-0216-7.

[25] C. Dong, C. C. Loy, K. He, and X. Tang, "Image super-resolution using deep convolutional networks," *IEEE Trans. Pattern Anal. Mach. Intell.*, vol. 38, no. 2, pp. 295–307, Feb. 2016, doi: 10.1109/TPAMI.2015.2439281.

[26] L. Zhang et al., "Adaptive importance learning for improving lightweight image super-resolution network," *Int. J. Comput. Vis.*, vol. 128, no. 2, pp. 479–499, Feb. 2020, doi: 10.1007/s11263-019-01253-6.

[27] Y. Zhang, K. Li, K. Li, L. Wang, B. Zhong, and Y. Fu, "Image super-resolution using very deep residual channel attention networks," in *Proc. Eur. Conf. Comput. Vis. (ECCV)* (Lecture Notes in Computer Science), vol. 11211, 2018, pp. 294–310, doi: 10.1007/978-3-030-01234-2_18.

[28] D. Song, Y. Wang, H. Chen, C. Xu, C. Xu, and D. Tao, "AdderSR: Towards energy efficient image super-resolution," in *Proc. IEEE/CVF Conf. Comput. Vis. Pattern Recognit. (CVPR)*, Jun. 2021, pp. 15643–15652.

[29] P. Isola, J.-Y. Zhu, T. Zhou, and A. A. Efros, "Image-to-image translation with conditional adversarial networks," in *Proc. IEEE Conf. Comput. Vis. Pattern Recognit. (CVPR)*, Jul. 2017, pp. 5967–5976, doi: 10.1109/CVPR.2017.632.

[30] Y. Chen, J. Xiong, W. Xu, and J. Zuo, "A novel online incremental and decremental learning algorithm based on variable support vector machine," *Cluster Comput.*, vol. 22, no. S3, pp. 7435–7445, May 2019, doi: 10.1007/s10586-018-1772-4.

[31] R. Lan, L. Sun, Z. Liu, H. Lu, C. Pang, and X. Luo, "MADNet: A fast and lightweight network for single-image super resolution," *IEEE Trans. Cybern.*, vol. 51, no. 3, pp. 1443–1453, Mar. 2021, doi: 10.1109/TCYB.2020.2970104.

[32] L. C. Chen, G. Papandreou, I. Kokkinos, K. Murphy, and A. L. Yuille, "Semantic image segmentation with deep convolutional nets and fully connected CRFs," in *Proc. 3rd Int. Conf. Learn. Represent. (ICLR)*, 2015, vol. 40, no. 4, pp. 834–848.

[33] A. Krizhevsky, I. Sutskever, and G. E. Hinton, "ImageNet classification with deep convolutional neural networks," *Commun. ACM*, vol. 60, no. 6, pp. 84–90, May 2017.

[34] B. Lim, S. Son, H. Kim, S. Nah, and K. M. Lee, "Enhanced deep residual networks for single image super-resolution," in *Proc. IEEE Conf. Comput. Vis. Pattern Recognit. Workshops (CVPRW)*, Jul. 2017, pp. 1132–1140, doi: 10.1109/CVPRW.2017.151.

[35] C. Qiao et al., "Evaluation and development of deep neural networks for image super-resolution in optical microscopy," *Nature Methods*, vol. 18, no. 2, pp. 194–202, Feb. 2021, doi: 10.1038/s41592-020-01048-5.

[36] W.-S. Lai, J.-B. Huang, N. Ahuja, and M.-H. Yang, "Fast and accurate image super-resolution with deep Laplacian pyramid networks," *IEEE Trans. Pattern Anal. Mach. Intell.*, vol. 41, no. 11, pp. 2599–2613, Nov. 2019, doi: 10.1109/TPAMI.2018.2865304.

[37] Y. Gao, L. Gao, and X. Li, "A generative adversarial network based deep learning method for low-quality defect image reconstruction and recognition," *IEEE Trans. Ind. Informat.*, vol. 17, no. 5, pp. 3231–3240, May 2021, doi: 10.1109/TII.2020.3008703.

[38] Hsien-I. Lin and F. S. Wibowo, "Image data assessment approach for deep learning-based metal surface defect-detection systems," *IEEE Access*, vol. 9, pp. 47621–47638, 2021, doi: 10.1109/ACCESS.2021.3068256.

[39] C. Lv, F. Shen, Z. Zhang, D. Xu, and Y. He, "A novel pixel-wise defect inspection method based on stable background reconstruction," *IEEE Trans. Instrum. Meas.*, vol. 70, pp. 1–13, 2021, doi: 10.1109/TIM.2020.3038413.

[40] N. Laroche, E. Carcreff, S. Bourguignon, J. Idier, A. Duclos, and P.-E. Lhuillier, "Detection and separation of close flaws in coarse-grained materials using ultrasonic image deconvolution," *J. Nondestruct. Eval.*, vol. 41, no. 4, p. 66, Dec. 2022, doi: 10.1007/s10921-022-00900-2.

[41] K. Zhang, W. Zuo, Y. Chen, D. Meng, and L. Zhang, "Beyond a Gaussian denoiser: Residual learning of deep CNN for image denoising," *IEEE Trans. Image Process.*, vol. 26, no. 7, pp. 3142–3155, Jul. 2017, doi: 10.1109/TIP.2017.2662206.

[42] W. Zhao et al., "Sparse deconvolution improves the resolution of live-cell super-resolution fluorescence microscopy," *Nature Biotechnol.*, vol. 40, no. 4, pp. 606–617, Apr. 2022, doi: 10.1038/s41587-021-01092-2.

[43] H. Wang et al., "Deep learning enables cross-modality super-resolution in fluorescence microscopy," *Nature Methods*, vol. 16, no. 1, pp. 103–110, Jan. 2019, doi: 10.1038/s41592-018-0239-0.

[44] I. Goodfellow et al., "Generative adversarial networks," *Commun. ACM*, vol. 63, no. 11, pp. 139–144, Oct. 2020, doi: 10.1145/3422622.

[45] E. Nehme, L. E. Weiss, T. Michaeli, and Y. Shechtman, "Deep-STORM: Super-resolution single-molecule microscopy by deep learning," *Optica*, vol. 5, no. 4, p. 458, 2018, doi: 10.1364/optica.5.000458.

[46] Z. H. Shah et al., "Deep-learning based denoising and reconstruction of super-resolution structured illumination microscopy images," *Photon. Res.*, vol. 9, no. 5, p. B168, 2021, doi: 10.1364/prj.416437.

[47] C. Liu, S. Xu, Y. Liu, and Z. Xiao, "Aperture design for a dark-field wafer defect inspection system," *Appl. Opt.*, vol. 60, no. 35, p. 10830, 2021, doi: 10.1364/ao.443118.

[48] F. Wang et al., "Residual attention network for image classification," in *Proc. IEEE Conf. Comput. Vis. Pattern Recognit. (CVPR)*, Jul. 2017, pp. 6450–6458, doi: 10.1109/CVPR.2017.683.

[49] Y. Wei, H. Xiao, H. Shi, Z. Jie, J. Feng, and T. S. Huang, "Revisiting dilated convolution: A simple approach for weakly- and semi-supervised semantic segmentation," in *Proc. IEEE/CVF Conf. Comput. Vis. Pattern Recognit.*, Jun. 2018, pp. 7268–7277, doi: 10.1109/CVPR.2018.00759.

[50] S. Mehta, M. Rastegari, A. Caspi, L. Shapiro, and H. Hajishirzi, *ESPNet: Efficient Spatial Pyramid of Dilated Convolutions for Semantic Segmentation* (Lecture Notes in Computer Science), vol. 11214, 2018, pp. 561–580, doi: 10.1007/978-3-030-01249-6_34.

[51] P. Liu, H. Zhang, J. Wang, Y. Wang, D. Ren, and W. Zuo, "Robust deep ensemble method for real-world image denoising," *Neurocomputing*, vol. 512, pp. 1–14, Nov. 2022, doi: 10.1016/j.neucom.2022.09.058.

[52] T. F. Crimmins, "Wafer noise models for defect inspection," in *Proc. 25th Metrol., Inspection, Process Control Microlithography*, vol. 7971, Apr. 2011, Art. no. 79710E, doi: 10.1117/12.879477.

Xuefeng Sun received the B.E. degree in biomedical engineering and the M.E. degree in instrument and meter engineering from the Changchun University of Science and Technology, Changchun, China, in 2017 and 2020, respectively. He is currently pursuing the Ph.D. degree in mechanical engineering with the Harbin Institute of Technology, Harbin. His research interests include digital image processing, machine learning, and design of microscope systems.

Baoyuan Zhang received the B.E. degree in technique and instrumentation of measurements from the Wuhan University of Technology, Wuhan, China, in 2019. She is currently pursuing the Ph.D. degree in instrument science and technology with the Harbin Institute of Technology, Harbin. Her research interests include optical design, digital image processing, and design of microscope systems.

Yushan Wang is currently pursuing the B.E. degree in instrument science and technology with the Harbin Institute of Technology, Harbin, China. Her current research interests include imaging of harmonic microscopy and optical system design.

Jialuo Mai is currently pursuing the B.E. degree in instrument science and technology with the Harbin Institute of Technology, Harbin, China. His current research interests include adaptive optics and optical system design.

Yuhang Wang received the B.E. degree in optical information engineering and the M.E. and Ph.D. degrees in instrument science and technology from the Harbin Institute of Technology, Harbin, China, in 2008, 2010, and 2016, respectively.

He has been with the College of Mechanical and Electrical Engineering, Northeast Forestry University, Harbin, where he is currently an Associate Professor. His current research interests include optical sensing technology, optical precision measurement technology, and instruments.

Jiubin Tan received the B.E., M.E., and Ph.D. degrees in instrument science and technology from the Harbin Institute of Technology, Harbin, China, in 1982, 1987, and 1991, respectively.

He has been with the Institute of Ultra-Precision Optoelectronic Instrument Engineering, Harbin Institute of Technology, where he is currently a Professor. He had published more than 310 refereed articles. His current research interests include ultra-precision measurement technology and instrument engineering, photoelectric imaging technology and instrument engineering, laser measurement technology and instruments, ultra-precision engineering, and equipment.

Weibo Wang received the B.E. and Ph.D. degrees in instrument science and technology from the Harbin Institute of Technology, Harbin, China, in 2005 and 2011, respectively.

He has been with the Institute of Ultra-Precision Optoelectronic Instrument Engineering, Harbin Institute of Technology, where he is currently a Professor. His current research interests include intelligent visual perception technology, design of microscope systems, intelligent sensing and imaging technology, and calculate the imaging.